

## CFD-DEM SIMULATION OF GAS FLUIDIZATION OF ELLIPSOIDAL PARTICLES

Z.Y. ZHOU<sup>1\*</sup>, D. PINSON<sup>2</sup>, R.P. ZOU<sup>1</sup> and A.B. YU<sup>1</sup>

<sup>1</sup>Laboratory for Simulation and Modelling of Particulate Systems, School of Materials Science and Engineering, The University of New South Wales, Sydney, NSW 2052, Australia

<sup>2</sup>BlueScope Steel Research, P.O. Box 202, Port Kembla, NSW 2505, Australia

\*Corresponding author, E-mail address: z.zhou@unsw.edu.au

### ABSTRACT

Fluidization is widely used in industries and has been extensively studied, experimentally and mathematically, in the past decades. In recent years, a coupled simulation approach of discrete element method (DEM) and computational fluid dynamics (CFD) has been successfully developed to study the gas-solid flow and heat transfer in fluidization at a particle scale. To date, such studies mainly deal with spherical particles. In this work, the CFD-DEM approach is extended to consider the fluidization of ellipsoidal particles. In the simulation, the particles used are either oblate or prolate. The commonly used correlations to determine the fluid drag acting on a non-spherical particle are compared. The effect of ellipsoid aspect ratio on the flow pattern, the relationship between pressure drop and gas superficial velocity, and particle orientations are investigated. It is shown that particle shape and orientation are important parameters in the study of gas fluidization.

### INTRODUCTION

Fluidization is widely used in many industries and has been extensively studied, experimentally and mathematically in the past decades. Generally, two approaches are available for mathematical modelling of the particulate phase: continuum at a macroscopic level and discrete at a microscopic level. Continuum modelling, based on local average principles, has been widely used in gas fluidization (for example, Anderson and Jackson, 1967; Gidaspow, 1994). However, its effective use depends on reliable constitutive or closure relations that are generally not available yet. Alternatively, discrete simulation, based on the analysis of the motion of individual particles, can overcome this difficulty, particularly, the application of the combined approach of CFD-DEM (computational fluid dynamics-discrete element method), as recently reviewed by Zhu et al. (2008). This approach can generate detailed dynamic information such as particle trajectories and transient forces acting on individual particles that are extremely difficult, if not impossible, to obtain experimentally. Capture of such information is important to depict the particle-particle and particle-fluid interactions and hence understand the fundamentals of particle-fluid flow under different conditions.

However, to date, the particles dealt with in the CFD-DEM modelling of fluidization are spherical particles, which cannot fully represent the practical particulate

systems. In practise, most natural particles are non-spherical, varying from regular to irregular shapes. Particle shape is one of the most important parameters of particle properties, and it affects the packing/flow structures that are critical to transport properties such as permeability related to pore connection and thermal conductivity related to particle connection. Techniques for DEM modelling of non-spherical particles have been reported in the literature, for example, as reviewed by Dziugys and Peters (2001). The main difficulties in addressing non-spherical particles are contact detection and force computation especially irregular shaped particles. For regular shapes such as ellipsoidal, cylindrical or cubic, analytical functions can be used to describe particle shape directly. In this study, ellipsoids are chosen as representative of a large number of particle shapes, for example, from prolate to oblate. Researchers have previously modelled ellipsoidal particles using DEM, for example (Rothenburg and Bathurst, 1991; Ting, 1992; Ting et al., 1993; Lin and Ng, 1995 and 1997; Vu-Quoc et al., 2000). However combination with fluid flow has not been considered in the literature.

In this work, the combined CFD-DEM approach is extended to consider the fluidization of ellipsoidal particles. In the simulation, particles used are either oblate or prolate. Due to the unavailability of drag correlations to reliably and accurately determine the fluid drag for non-spherical particles, the commonly used correlations in the literature are compared, and an appropriate one is chosen for the current CFD-DEM simulation. The effect of the aspect ratio of ellipsoids on the flow pattern, the relationship between pressure drop and gas superficial velocity, and particle orientations are investigated.

### MODEL DESCRIPTION

#### DEM for ellipsoidal particles

The particle phase mode is based on the soft sphere DEM model originally proposed by Cundall and Strack (1979). The governing equations for the translational and rotational motion of particle  $i$  with radius  $R_i$ , mass  $m_i$  and moment of inertia  $I_i$  can be written as:

$$m_i d\mathbf{v}_i / dt = \mathbf{f}_{pf,i} + \sum_{j=1}^{k_c} (\mathbf{F}_{c,ij} + \mathbf{F}_{d,ij}) + m_i \mathbf{g} \quad (1)$$

$$I_i d\boldsymbol{\omega}_i / dt = \sum_{j=1}^{k_c} \mathbf{M}_{ij} \quad (2)$$

where  $\mathbf{v}_i$  and  $\boldsymbol{\omega}_i$  are the translational and angular velocities of the particle, respectively, and  $k_c$  is the number of particles in interaction with the particle. As shown in Figure 1, the forces involved are: particle-fluid interaction

force  $\mathbf{f}_{pf,i}$ , the gravitational force  $m_i\mathbf{g}$ , and inter-particle forces which include elastic force  $\mathbf{F}_{c,ij}$  and viscous damping force  $\mathbf{F}_{d,ij}$ . The torques acting on particle  $i$  by particle  $j$  include:  $\mathbf{M}_{r,ij}$  generated by tangential force,  $\mathbf{M}_{t,ij}$  commonly known as the rolling friction torque, and also the torque generated by normal force. This is because normal force does not necessarily pass through the centre of ellipsoids. The equations used to calculate the particle-particle interaction forces in this work are the same as those for spherical particles that have been well established in the literature, for example, as discussed by Zhu et al. (2007). For convenience, their expressions are listed in Table 1.

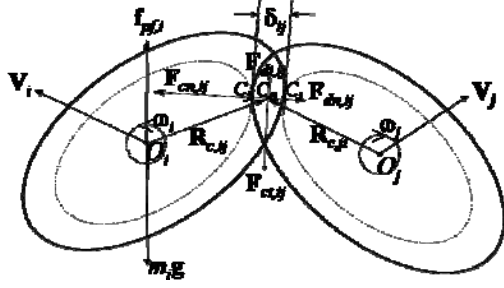


**Figure 1:** Two-dimensional illustration of the forces acting particle  $i$  in contact with particle  $j$ .

A key feature of DEM modelling for non-spherical particles is determination of the particle orientation in addition to more complicated contact detection. Various analytical methods of contact detection for two- and three-dimensional elliptical particles have been proposed in the literature by intersection algorithm (Rothenburg and Bathurst, 1991), geometric potential algorithm (Ting, 1992; Lin and Ng, 1995), or common normal algorithm (Lin and Ng, 1995). In the present work, the so-called geometric potential algorithm is used. As shown in Figure 1, contact location point  $C_{ij}$  is defined as the midpoint of the line connecting the ‘‘touch’’ points  $C_i$  and  $C_j$ , where  $C_i$  is defined as the ‘‘deepest’’ point of ellipsoid  $i$  inside ellipsoid  $j$  and  $C_j$  as the ‘‘deepest’’ point of ellipsoid  $j$  inside ellipsoid  $i$ . More details of the determination of touch points  $C_i$  and  $C_j$  can be found elsewhere (for example, Lin and Ng, 1995).

The orientations of the particle’s principal axes can be described by three Euler angles  $(\phi, \theta, \psi)$  (Goldstein, 1980). For convenience the inertia tensor  $\mathbf{I}_i$  in Eq. (2) defined in the space-fixed coordinate system  $(x, y, z)$  is converted to the body-fixed coordinate system  $(x', y', z')$  by a transformation matrix  $\mathbf{A}$ , determined by three Euler angles (Goldstein, 1980). The body-fixed coordinate system is a moving Cartesian coordinate system, which is fixed with the particle and whose axes are superposed by the principle axes of inertia (Rahman and Stiller, 1971). Then the inertia tensor always is diagonal  $I_i = (I_{i,x'}, I_{i,y'}, I_{i,z'})$ . Thus, Eq. (2) in the body-fixed coordinate system can be re-written as

$$I_{i,x'} d\omega_{i,x'}^b / dt - \omega_{i,y'}^b \omega_{i,z'}^b (I_{i,y'} - I_{i,z'}) = M_{ij,x'}^b \quad (3)$$

$$I_{i,y'} d\omega_{i,y'}^b / dt - \omega_{i,z'}^b \omega_{i,x'}^b (I_{i,z'} - I_{i,x'}) = M_{ij,y'}^b \quad (4)$$

$$I_{i,z'} d\omega_{i,z'}^b / dt - \omega_{i,x'}^b \omega_{i,y'}^b (I_{i,x'} - I_{i,y'}) = M_{ij,z'}^b \quad (5)$$

where superscript  $b$  indicates that the parameter is defined in the body-fixed coordinate system. Thus, the angular

velocities  $(\omega_{i,x'}^b, \omega_{i,y'}^b, \omega_{i,z'}^b)$  of particles can be calculated in the body-fixed system by Eqs. (3-5).

Angular velocities  $(\omega_{i,x'}^b, \omega_{i,y'}^b, \omega_{i,z'}^b)$  are closely related to the changes of Euler angles, and their relations can be written as

$$\omega_{i,x'}^b = d\phi / dt \sin \theta \sin \psi + d\theta / dt \cos \psi \quad (6)$$

$$\omega_{i,y'}^b = d\phi / dt \sin \theta \cos \psi - d\theta / dt \sin \psi \quad (7)$$

$$\omega_{i,z'}^b = d\phi / dt \cos \theta + d\psi / dt \quad (8)$$

Thus, three Euler angles can be calculated by Eqs. (6-8), then the spatial orientation of particles is determined. In the present work the quaternion method is used. The details of which can be found elsewhere (for example, Goldstein, 1980).

### CFD for fluid phase

The motion of the continuum fluid is calculated from the Navier-Stokes and continuity equations based on local mean variables over a computational cell, which can be written as

$$\partial \varepsilon_f / \partial t + \nabla \cdot (\varepsilon_f \mathbf{u}) = 0 \quad (9)$$

$$\partial (\rho_f \varepsilon_f \mathbf{u}) / \partial t + \nabla \cdot (\rho_f \varepsilon_f \mathbf{u} \mathbf{u}) = -\nabla p - \left( \sum_{i=1}^{k_v} \mathbf{f}_{pf,i} \right) / \Delta V + \nabla \cdot \varepsilon_f \boldsymbol{\tau} + \rho_f \varepsilon_f \mathbf{g} \quad (10)$$

where  $\mathbf{u}$ ,  $\rho_f$ , and  $p$  are the fluid velocity, density, pressure, respectively, and  $k_v$  is the number of particles in a computational cell of volume  $\Delta V$ . Particle-fluid interaction force  $\mathbf{f}_{pf,i}$  considered in the present work includes pressure gradient force and drag force as listed in Table 1.  $\boldsymbol{\tau}$  and  $\varepsilon_f$  are the fluid viscous stress tensor and porosity, respectively, which are given as  $\boldsymbol{\tau} = \mu_e [(\nabla \mathbf{u}) + (\nabla \mathbf{u})^T]$  and  $\varepsilon_f = 1 - \sum_{i=1}^{k_v} V_i / \Delta V$ , respectively.  $V_i$  is the volume of particle  $i$  (or part of the volume if the particle is not fully in the cell),  $\mu_e$  the fluid effective viscosity determined by the standard  $k-\varepsilon$  turbulent model as used elsewhere (Zhang et al., 1998; Zhou et al., 2009).

### Drag force for non-spherical particles

Determination of fluid drag acting on non-spherical particles has been addressed in the literature. For example, the Ergun equation (1952) considered the effect of particle shape by sphericity  $(\phi)$ , but at a macroscopic scale. Some reviews on the fluid drag for non-spherical particles have been made (Ganser, 1993; Loth, 2008). Haider and Levenspiel (1989) established a four-parameter correlation for drag coefficient  $C_D$ , but ignored the effect of orientation. Ganser (1993) proposed a drag correlation using correction factors (Stokes factor and Newton’s factor), and claimed that it is general and also accurate to determine  $C_D$ . Holzer and Sommerfeld (2008) used literature data and proposed a new correlation of  $C_D$  with the consideration of both the shape and the orientation. Table 1 lists those correlations, and their quantitative comparison will be made later. It should be noted that the scheme proposed by Di Felice (1994), which has been widely used in the CFD-DEM modelling for spherical particles, is assumed still valid for non-spherical particles and used in the present work.

The CFD-DEM coupling methodology has been well documented elsewhere (for example, Xu and Yu, 1997; Feng and Yu, 2004), and hence only briefly described here. At each time step, DPS will give information such as

the positions and velocities of individual particles. From these, the porosity and volumetric fluid-particle interaction force in each computational cell are calculated. CFD will then use the information to determine the gas

flow field, from which the fluid drag forces acting on individual particles are calculated. Incorporation of the resulting forces into DPS produces information about the motion of the individual particles for the next time step.

**Table 1:** Components of forces and torque acting on particle  $i$

Forces	Correlations
Normal elastic force	$-4/3E^*\sqrt{R^*}\delta_n^{3/2}\mathbf{n}$
Normal damping force	$-c_n\left(8m_{ij}E^*\sqrt{R^*}\delta_n\right)^{1/2}\mathbf{V}_{n,ij}$
Tangential elastic force	$-\mu_s \mathbf{F}_{cn,ij} \left(1-(1-\delta_t/\delta_{t,max})^{3/2}\right)\hat{\delta}_t$ ( $\delta_t < \delta_{t,max}$ )
Tangential damping force	$-c_t\left(6\mu_s m_{ij} \mathbf{F}_{cn,ij} \sqrt{1- \mathbf{v}_t /\delta_{t,max}}/\delta_{t,max}\right)^{1/2}\mathbf{V}_{t,ij}$ ( $\delta_t < \delta_{t,max}$ )
Coulumb friction force	$-\mu_s \mathbf{F}_{cn,ij} \hat{\delta}_t$ ( $\delta_t \geq \delta_{t,max}$ )
Torque by tangential forces	$\mathbf{R}_{c,ij} \times (\mathbf{F}_{ct,ij} + \mathbf{F}_{dt,ij})$
Torque by normal force	$\mathbf{R}_{c,ij} \times (\mathbf{F}_{cn,ij} + \mathbf{F}_{dn,ij})$
Rolling friction torque	$\mu_r \mathbf{F}_{n,ij} \hat{\omega}_{t,ij}^n$
	<p>where <math>R^*</math> is the reduced radius of the particle <math>i</math> and <math>j</math> at the contact point, and defined as <math>R^* = 1/2\sqrt{A'B'}</math> and <math>A', B'</math> are related to the radii of the particle shape curvature at contact point (Dziugys and Peters, 2001), <math>1/m_{ij} = 1/m_i + 1/m_j</math>, <math>E^* = E/2(1-\nu^2)</math>,</p> <p><math>\hat{\omega}_{t,ij} = \boldsymbol{\omega}_{t,ij}/ \boldsymbol{\omega}_{t,ij} </math>, <math>\hat{\delta}_t = \delta_t/ \delta_t </math>, <math>\delta_{t,max} = \mu_s(2-\nu)/2(1-\nu)\delta_n</math>,</p> <p><math>\mathbf{V}_{ij} = \mathbf{V}_j - \mathbf{V}_i + \boldsymbol{\omega}_j \times \mathbf{R}_{c,ji} - \boldsymbol{\omega}_i \times \mathbf{R}_{c,ij}</math>, <math>\mathbf{V}_{n,ij} = (\mathbf{V}_{ij} \cdot \mathbf{n}) \cdot \mathbf{n}</math>, <math>\mathbf{V}_{t,ij} = (\mathbf{V}_{ij} \times \mathbf{n}) \times \mathbf{n}</math>. Note that tangential forces (<math>\mathbf{F}_{ct,ij} + \mathbf{F}_{dt,ij}</math>) should be replaced by <math>\mathbf{F}_{t,ij}</math> when <math>\delta_t \geq \delta_{t,max}</math>.</p>
Pressure gradient force	$-\nabla p \cdot V_p$
Drag force	<p><u>Ergun equation (1952):</u></p> $F_d = \frac{V_p \beta}{1 - \varepsilon_f}  \mathbf{u} - \mathbf{v}  (\mathbf{u} - \mathbf{v}) \quad \text{and} \quad \beta = a \frac{\mu_f (1 - \varepsilon_f)^2}{\varepsilon_f (\varphi d_v)^2  \mathbf{u} - \mathbf{v} } + b \frac{\rho_f (1 - \varepsilon_f)^2}{\varepsilon_f (\varphi d_v)} \quad (a = 150, b = 1.75)$ <p><u>Scheme by Di Felice (1994):</u></p> $\mathbf{F}_{f,i} = 0.125 C_D \rho_f \pi d_v^2 \varepsilon_f^2  \mathbf{u}_i - \mathbf{v}_i  (\mathbf{u}_i - \mathbf{v}_i) \cdot \varepsilon_i^{-\chi} \quad \chi = 3.7 - 0.65 \exp[-(1.5 - \log_{10} Re_i)^2 / 2]$ <p>where <math>d_v</math> is the volume-equivalent particle diameter, <math>d_v = 2(abc)^{1/3}</math> (<math>a, b</math> and <math>c</math> are three principle radii of an ellipsoidal particle), <math>Re_i = \rho_f d_v \varepsilon_f  \mathbf{u}_i - \mathbf{v}_i  / \mu_f</math>, and <math>C_D</math> is the drag coefficient which can be determined by different correlations:</p> <p><i>Haider &amp; Levenspiel (1989):</i> <math>C_D = \frac{24}{Re} (1 + A Re^B) + \frac{C}{1 + D/Re}</math></p> <p><i>Ganser (1993):</i> <math>\frac{C_D}{K_2} = \frac{24}{Re K_1 K_2} (1 + 0.1118 (Re K_1 K_2)^{0.6567}) + \frac{0.4305}{1 + 3305/Re K_1 K_2}</math></p> <p><i>Holzer &amp; Sommerfeld (2008):</i> <math>C_D = \frac{8}{Re} \frac{1}{\sqrt{\varphi_{  }}} + \frac{16}{Re} \frac{1}{\sqrt{\varphi_{\perp}}} + \frac{3}{\sqrt{Re}} \frac{1}{\varphi^{3/4}} + 0.42 \cdot 10^{0.4(-\log \varphi)^{0.2}} \frac{1}{\varphi_{\perp}}</math></p> <p>where <math>K_1, K_2</math> are correction factors for Stokes flow and Newton's flow regions, respectively. <math>\varphi</math> is the particle sphericity defined as the ratio of surface area of a sphere being equivalent volume of the ellipsoid to the surface area of the ellipsoid, <math>\varphi_{\perp}</math> is crosswise sphericity, and <math>\varphi_{  }</math> is lengthwise sphericity. More details of <math>\varphi_{\perp}</math> and <math>\varphi_{  }</math> can be referred to Holzer &amp; Sommerfeld (2008).</p>

## SIMULATION CONDITIONS

A two-dimensional slot model with wall boundary conditions was used in this study. For such geometry, two-dimensional CFD and three-dimensional DEM solutions are used as elsewhere (for example, Feng et al., 2004). The bed was generated under the so-called poured packing conditions (Zhang et al., 2001). Uniform ellipsoids were poured from a certain height, with randomly generated initial velocities and orientations. During this process, ellipsoids may collide each other, and bounce back and

forth while colliding with the walls. The dynamic process proceeds until all ellipsoids reach their stable positions. The bed is then fluidized by gas uniformly introduced from the bottom. Table 2 lists DEM parameters, physical properties of particles and fluid used in the simulation. It should be noted that two types of particles were modelled: plastic ellipsoidal particles as used in the experimental work by Wu (2001), and chocolate candies with different shapes.

**Table 2:** Various parameters used in the simulation

	Variables	Values
DEM parameters	Sliding friction, $\mu_s$	0.3
	Rolling friction, $\mu_r$	$0.01d_v$
	Young's modulus, $E$	$1 \times 10^7 \text{ kg}/(\text{m} \cdot \text{s}^2)$
	Poisson ratio, $\nu$	0.3
	Time step, $\Delta t$	$3.696 \times 10^{-5} \text{ s}$
Plastic particles	Width $\times$ thickness $\times$ height (x, y, z)	$120 \times 33 \times 130 \text{ mm}$
	CFD cells (x, z)	$10 \times 30 \text{ cells}$
	Number of particles, N	12,000
	Size ( $2a \times 2b \times 2c$ , $d_v$ )	$1.682 \times 5.5 \times 5.5 \text{ mm}$ $d_v = 3.7 \text{ mm}$
	Density	$950 \text{ kg}/\text{m}^3$
	Sphericity, $\phi$	0.764
Chocolate candies	Width $\times$ thickness $\times$ height (x, y, z)	$300 \times 50 \times 320 \text{ mm}$
	CFD cells (x, z)	$10 \times 60 \text{ cells}$
	Particle size ( $d_v$ )	8.634 mm
	Density	$1439 \text{ kg}/\text{m}^3$
Gas properties	Density	$1.2 \text{ kg}/\text{m}^3$
	Viscosity	$1.8 \times 10^{-5} \text{ Pa} \cdot \text{s}$

## RESULTS & DISCUSSION

The four non-spherical drag force correlations given in Table 1 were qualitatively compared in the CFD-DEM model under the conditions listed in Table 2. The a and b Ergun equation parameters use the recommended values from Wu et al. (2001) to match their experimentally obtained data for plastic particles, 102.93 and 2.5 respectively. The obtained pressure drop with gas superficial velocity is shown in Figure 2. It can be observed that there is no significant difference except the model by Ganser (1993), indicating that other four correlations all can be used in the CFD-DEM modelling. However, it should be noted that Ergun equation/modified Ergun equation is based on the macroscopic scale to determine the drag while the correlation of (Haider and Levenspiel, 1989) does not consider the effect of particle orientation. Thus, the correlation by Holzer and Sommerfeld (2008), which considers the effects of both shape and orientation, is more preferable, and will be used in the later simulation cases.

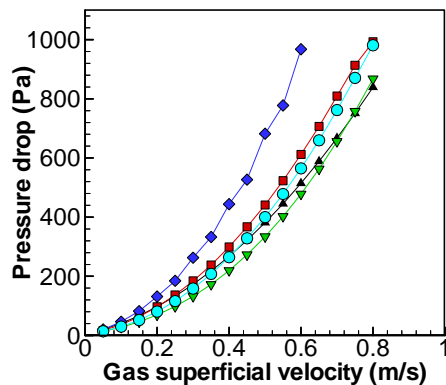


**Figure 2:** Pressure drop with gas superficial velocities for different drag correlations:  $\Delta$ , Ergun equation (1952);  $\square$ , Modified Ergun equation (Wu, 2001);  $\nabla$ , Haider and Levenspiel (1989);  $\diamond$ , Ganser (1993); and  $\circ$ , Holzer and Sommerfeld (2008).

Particle shape is one important property of particles, and it significantly affects the particle-particle connection and consequently the packing structure. In the simulation, in

order to examine the effect of particle shape, ellipsoidal particles with five different aspect ratios but having the same volumes are used. The particles used are chocolate candies and their properties are listed in Table 2. Figure 3 shows the generated bed structures, and Table 3 lists their properties. It can be seen that bed with spherical particles has the highest porosity and the least particle-particle contact number. Beds with prolate/oblate particles have a lower porosity and higher particle-particle contact number, indicating the more dense packing structure for ellipsoidal particles, which is consistent with the reported (for example, Zou and Yu, 1996).

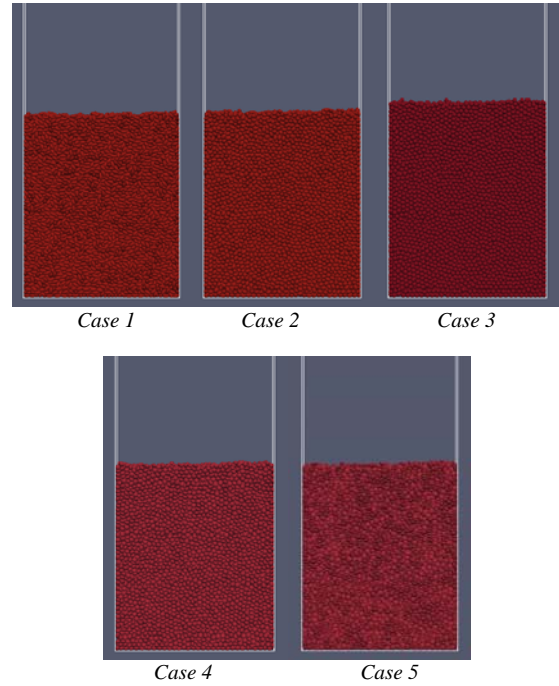


**Figure 3:** Bed structures of ellipsoids with different aspect ratios, and their properties are shown in Table 3.

**Table 3:** Bed properties shown in Figure 3

Properties	Case 1	Case 2	Case 3	Case 4	Case 5
Shape	Prolate	Prolate	Spherical	Oblate	Oblate
Particle number	10000	10000	10000	10000	10000
Size (mm) ( $2a, 2b, 2c$ )	13.4	10.459	8.634	7.1265	5.439
( $d_v = 8.634$ )	6.93	7.844	8.634	9.502	10.878
	6.93	7.844	8.634	9.502	10.878
Aspect ratio ( $\eta = a/b$ )	1.933	1.333	1.0	0.75	0.5
Sphericity	0.935	0.986	1.0	0.985	0.912
Bed porosity	0.354	0.363	0.396	0.365	0.360
Contact number	295757	148624	70206	102759	160676

One of the most important advantages of CFD-DEM simulation is that the rich microscopic information can be readily obtained such as flow and force structures, which is very important to elucidate the underlying mechanisms of particle-fluid flow as demonstrated by Zhu et al. (2008). As an example, Figure 4 shows a snapshot with microscopic information for case 5 when gas superficial velocity is 2.6 m/s. Figure 4(a) and (b) show spatial distributions of particle-particle interaction force and particle-fluid interaction force, respectively, acting on each oblate spheroid. Figure 4(c) shows the spatial

distribution of particle orientation that is presented by a vector. The velocity vectors are shown in Figure 4(d). The obtained microscopic information is very useful to further examine the shape effect on the flow behavior of ellipsoids in a fluidized bed.

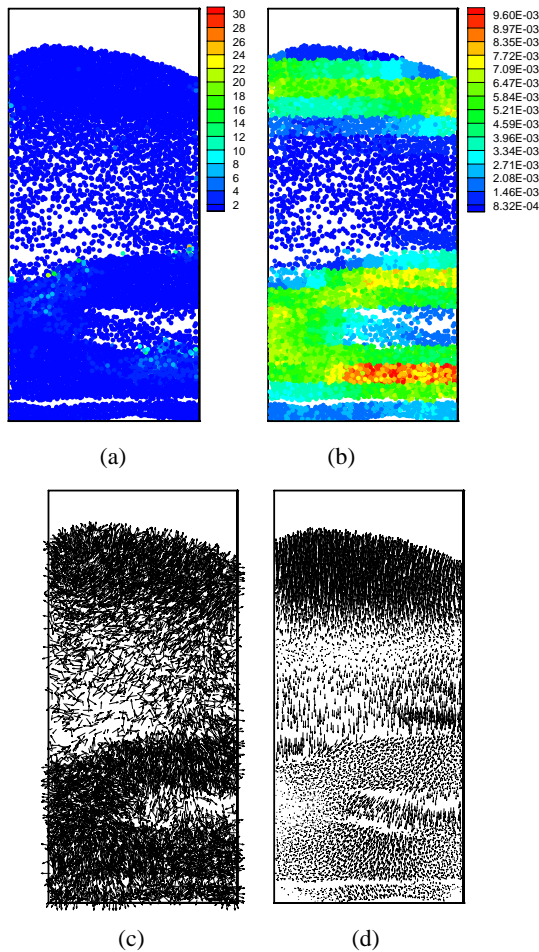


**Figure 4:** Microscopic information obtained for case 5 when  $U=2.6$  m/s: (a) particle-particle contact force, (b) particle-fluid interaction force, (c) vectors of particle orientation, and (d) vectors of particle velocity.

Particle orientations in a fluidized bed, as shown in Figure 4(c), can be further analyzed by angular distributions to examine the bed isotropy/anisotropy. As shown in Figure 5, the angle in the angular direction represents the longitude  $\alpha$  of the vector (shown in Figure 4c) on the basis of the equatorial planes being X-O-Y, or X-O-Z, or Y-O-Z, respectively, where axis of X, Y, Z are indicated in Table 2. Longitude  $0^\circ$  is defined at the positive axis of X or Y. The number of particles with similar longitudes ( $\Delta\alpha=3^\circ$ ) is counted, and its value is shown in radial direction. As shown in Figure 5(b), the distributions for spherical particles are isotropic. This is because spheres are isotropic, and as such the orientation is not significant. But for prolate particles, as shown in Figure 5(a), the vector which represents the direction of principle axis  $a$  (the longest radius of prolate spheroids) tends to be in the X horizontal direction not in the Y horizontal direction due to the confined space (small thickness of bed geometry). For oblate particles, the principle axis  $a$  (the shortest radius of oblate spheroids) tends to be in the vertical direction Z (Figure 5(c)), and the equatorial plane of oblate spheroids is preferred on the

X-O-Y plane. The angular distributions shown in Figure 5 indicate that beds with prolate or oblate spheroids are anisotropic. Such a feature of anisotropy could affect the performance of fluidized beds in its application.

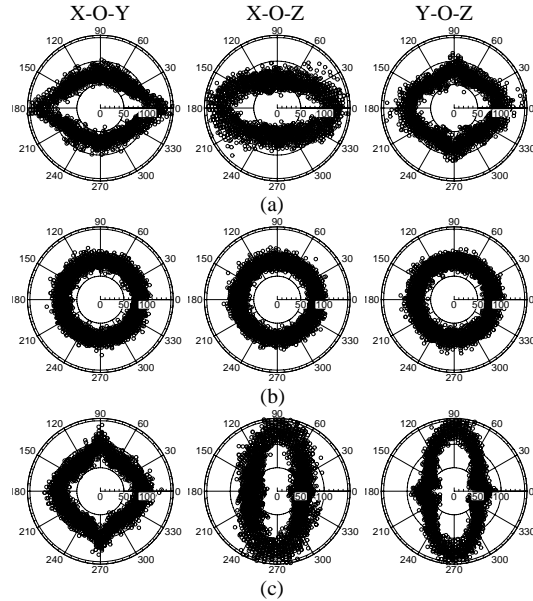


**Figure 5:** Angular distributions of particle orientations: (a) case 1, (b) case 3, and (c) case 5.

The correlation of pressure drop with gas superficial velocity is important to analyse the bed permeability. Figure 6 shows the correlations between the dimensionless pressure drop and gas superficial velocities for the simulated 5 cases. It can be observed that, in the fixed bed, under the same gas superficial velocity, a bed with spherical particles has the lowest pressure drop, indicating the highest permeability. This is consistent with the highest bed porosity shown in Table 3. With increasing or decreasing aspect ratio, the bed becomes denser. Correspondingly, the pressure drop increases. Characteristically the pressure drops in the fluidized bed regime for the five cases are similar to the bed weight indicating reliable model formulation. It also should be noted that the maximum pressure drop and their corresponding gas superficial velocities are different. Spherical particles begin to fluidize at higher gas superficial velocity while, with the sphericity decreasing, the corresponding gas superficial velocity decreases.

One of the most important reasons for the wide application of fluidized bed in industry is the rapid heat transfer between particle-fluid and particle-particle. Particle shape significantly affects particle-particle contact number, as shown in Table 3 for static beds. Figure 7 shows the variations of particle-particle contact number in fluidized beds for prolate (case 1) and oblate (case 5) spheroids, respectively. It can be seen that the particle-particle contact number for oblate is much less than that for prolate. Such a feature may be significant for the heat transfer behaviour in fluidized beds. High rates of particle-particle collisions for prolate particles may lead to increased particle-particle heat transfer. Both cases also show that, with increasing gas superficial velocity, the contact number decreases as mean particle separation increases.

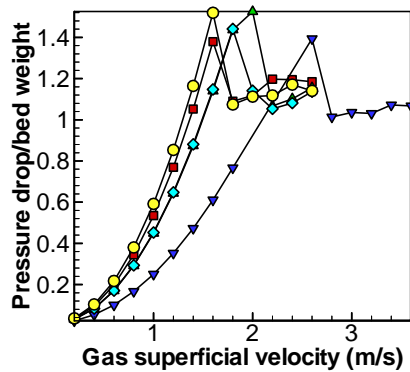


**Figure 6:** Dimensionless pressure drop with gas superficial velocities corresponding to Figure 3:  $\square$ , case 1;  $\Delta$ , case 2;  $\nabla$ , case 3;  $\diamond$ , case 4; and  $\circ$ , case 5).

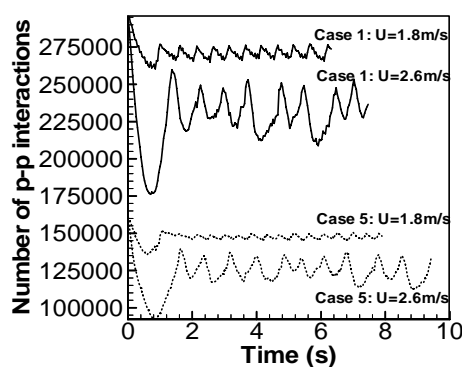


**Figure 7:** Number of particle-particle collisions in the fluidized beds of case 1 and case 5, respectively, for different gas superficial velocities.

## CONCLUSION

CFD-DEM modelling was extended in this work to study gas fluidization with ellipsoidal particles. The correlation of Holzer and Sommerfeld (2008) was used to determine the fluid drag. The effect of aspect ratio of ellipsoids on the flow pattern and the relationship between pressure drop and gas superficial velocity was investigated. It was shown that beds of ellipsoids with different aspect ratios have denser packing structures than spheres, which could significantly affect the flow behaviour. Examination of particle orientations showed that the bed structures are not isotropic, particularly when particle sphericity becomes smaller. Further qualitative comparison with experiments in terms of flow patterns and some parameters such as minimum fluidization velocity and the correlation of pressure drop and gas superficial velocity is required in the future work.

## ACKNOWLEDGEMENTS

The authors are grateful to Australian Research Council (ARC) and BlueScope Steel Research for the financial support of this work.

## REFERENCES

ANDERSON, T.B., JACKSON, R., (1967), "A fluid mechanical description of fluidized beds", *Industrial & Engineering Chemistry Fundamentals*, 6, 527-539.  
 CUNDALL, P.A., STRACK, O.D.L., (1979), "Discrete numerical model for granular assemblies", *Geotechnique*, 29, 47-65.

DI FELICE, R., (1994), "The voidage function for fluid-particle interaction systems", *International Journal of Multiphase Flow*, 20, 153-159.  
 DZIUGYS, A., PETERS, B., (2001), "An approach to simulate the motion of spherical and non-spherical fuel particles in combustion chambers", *Granular Matter*, 3, 231-265.  
 ERGUN, S., (1952), "Fluid flow through packed columns", *Chemical Engineering and Processing*, 48, 89-94.  
 FENG, Y.Q., YU, A.B., (2004), "Assessment of model formulations in the discrete particle simulation of gas-solid flow", *Industrial and Engineering Chemistry Research*, 43, 8378-8390.  
 GANSER, G.H., (1993), "A rational approach to drag prediction of spherical and nonspherical particles", *Powder Technol.*, 77, 143-152.  
 GIDASPOW, D., (1994), "Multiphase Flow and Fluidization", Academic Press, San Diego.  
 HAIDER, A., LEVENSPIEL, O., (1989), "Drag coefficient and terminal velocity of spherical and nonspherical particles", *Powder Technol.*, 58, 63-70.  
 HOLZER, A., SOMMERFELD, M., (2008), "New simple correlation formula for the drag coefficient of non-spherical particles", *Powder Technol.*, 184, 361-365.  
 LIN, X., NG, T.T., (1995), "Contact detection algorithms for three-dimensional ellipsoids in discrete element modelling", *International Journal for Numerical and Analytical Methods in Geomechanics*, 19, 653-659.  
 LIN, X., NG, T.T., (1997), "A three-dimensional discrete element model using arrays of ellipsoids", *Geotechnique*, 47, 319-329.  
 LOTH E., (2008), "Drag of non-spherical solid particles of regular and irregular shape", *Powder Technology*, 182, 342-353.  
 RAHMAN, A., STILLING, F.H., (1971), "Molecular dynamics study of liquid water", *Journal of Chemical Physics*, 55, 3336-&.  
 ROTHENBURG, L., BATHURST, R.J., (1991), "Numerical simulation of idealized granular assemblies with plane elliptical particles", *Computers and Geotechnics*, 11, 315-329.  
 TING, J.M., (1992), "A robust algorithm for ellipse-based discrete element modelling of granular material", *Computers and Geotechnics*, 13, 175-186.  
 TING, J.M., KHWAJA, M., MEACHUM, L., ROWELL, J.D., (1993), "An ellipse-based discrete element model for granular materials", *International Journal for Numerical and Analytical Methods in Geomechanics*, 17, 603-623.  
 GOLDSTEIN, H., (1980), "Classical Mechanics", Addison-Wesley Publishing Company.  
 VU-QUOC, L., ZHANG, X., WALTON, O.R., (2000), "A 3-D Discrete-Element Method for dry granular flows of ellipsoidal particles", *Computer Methods in Applied Mechanics and Engineering Journal*, 187, 483-528.  
 WU, S.M., (2001), Permeability and minimum fluidization velocity of non-spherical particle mixtures, Master Thesis, The University of New South Wales.  
 XU, B.H., YU, A.B., (1997), "Numerical simulation of the gas-solid flow in a fluidized bed by combining discrete particle method with computational fluid dynamics", *Chem. Eng. Sci.*, 52, 2785-2809.  
 ZHANG, S.J., YU, A.B., ZULLI, P., WRIGHT, B., TUZUN, U., (1998), "Modelling of the solids flow in a blast furnace", *ISIJ Int.*, 38, 1311-1319.  
 ZHANG, Z.P., LIU, L.F., YUAN, Y.D., YU, A.B., (2001), "A simulation study of the effects of dynamic variables on the packing of spheres", *Powder Technol.*, 116, 23-32.  
 ZHOU, Z.Y., YU, A.B., ZULLI, P., (2009), "Particle scale study of heat transfer in packed and bubbling fluidized beds", *AIChE*, 55, 868-884.  
 ZHU, H.P., ZHOU, Z.Y., YANG, R.Y., YU, A.B., (2008), "Discrete particle simulation of particulate systems: A review of major applications and findings", *Chem. Eng. Sci.*, 63, 5728-5770.  
 ZOU, R.P., YU, A.B., (1996), "Evaluation of the packing characteristics of mono-sized non-spherical particles", *Powder Technol.*, 88, 71-79.